The Astrophysical Journal Letters, 940:L17 (10pp), 2022 November 20 https://doi.org/10.3847/2041-8213/ac9b27

A First Look at Cepheids in a Type Ia Supernova Host with JWST

Wenlong Yuan[1], Adam G. Riess[1,2], Stefano Casertano[2], and Lucas M. Macri[3]
[1] Department of Physics & Astronomy, Johns Hopkins University, Baltimore, MD 21218, USA; wyuan10@jhu.edu
[2] Space Telescope Science Institute, 3700 San Martin Drive, Baltimore, MD 21218, USA
[3] George P. and Cynthia W. Mitchell Institute for Fundamental Physics and Astronomy, Department of Physics and Astronomy, Texas A&M University, College Station, TX 77843, USA
Received 2022 September 16; revised 2022 October 14; accepted 2022 October 18; published 2022 November 24

Abstract

We report the first look at extragalactic Cepheid variables with the James Webb Space Telescope (JWST), obtained from an archival observation of NGC 1365, host of SNIa 2012fr, a calibration path used to measure the Hubble constant. As expected, the high-resolution observations with NIRCam through F200W show better source separation from line-of-sight companions than Hubble Space Telescope (HST) images at similar near-infrared wavelengths, the spectral region that has been used to mitigate the impact of host dust on distance measurements. Using the standard star P330E as a zero-point and point-spread function reference, we photometered 31 previously known Cepheids in the JWST field, spanning $1.15 < \log P < 1.75$ including 24 Cepheids in the longer-period interval of $1.35 < \log P < 1.75$. We compared the resultant period–luminosity (P-L) relations to that of 49 Cepheids in the full period range including 38 in the longer-period range observed with WFC3/IR on HST and transformed to the JWST photometric system (F200W, Vega). The P-L relations measured are in good agreement, with intercepts (at $\log P = 1$) of 25.74 ± 0.04 and 25.72 ± 0.05 for HST and JWST, respectively. Our baseline result comes from the longer-period, higher signal-to-noise ratio Cepheids where we find 25.75 ± 0.05 and 25.75 ± 0.06 mag for HST and JWST, respectively. We find good consistency between this first JWST measurement and HST, and no evidence that HST Cepheid photometry is "biased bright" at the ∼0.2 mag level needed to mitigate the Hubble tension, though comparisons from more SN hosts are warranted and anticipated. We expect future optimized JWST observations to surpass these in quality.

Unified Astronomy Thesaurus concepts: Hubble constant (758); James Webb Space Telescope (2291); Cepheid distance (217); Cepheid variable stars (218)

1. Introduction

Cepheid variables have held a central role in measuring extragalactic distances for more than a century (Leavitt & Pickering 1912). They exhibit several features that make them uniquely suited for this role. Their nature is well understood as a consequence of the κ mechanism, which drives a periodic overshooting of hydrostatic equilibrium and produces their pulsations (Eddington 1927). Their great luminosities, $\sim 10^5 L_\odot$, make them visible with modern telescopes at many tens of Megaparsecs. The large amplitude of their variations uniquely identifies them, and their periods standardize their luminosities to a precision of a few percent. They are ubiquitous in areas of recent star formation, including many hosts of Type Ia supernovae (SNe Ia; which have still greater range). Finally, hundreds of Cepheids in the Milky Way (MW) are in range of precise parallaxes from the ESA Gaia satellite to provide a 1% geometric calibration of their fiducial luminosity (Riess et al. 2022a; Cruz Reyes & Anderson 2022). For these reasons, Cepheids are the primary distance indicator most often selected for measuring long-range distances and the Hubble constant (Riess et al. 2022b, hereafter R22).

A succession of technological advancements has extended the reach, precision, and accuracy of Cepheid distance estimates at tens of Megaparsecs. One of the original goals of the Hubble Space Telescope (HST) was to resolve extragalactic Cepheids, which was achieved in dozens of galaxies within ∼20 Mpc with the Wide Field Planetary Camera 2 (WFPC2) at optical wavelengths (Freedman et al. 2001; Sandage et al. 2006). HST instruments with greater sensitivity and higher resolution, ACS and WFC3/UVIS, extended this reach to ∼50 Mpc and a greater number of nearby SNe Ia and geometric calibrators (Macri et al. 2006; Riess et al. 2011; Hoffmann et al. 2016).

Given that Cepheids are found in regions of recent star formation, they are observed through interstellar dust with a mean reddening (in modestly inclined spirals; R22) of $E(V-I) \sim 0.3$ mag. Thus, their visible (0.5 μm) and infrared (0.8 μm) band measurements must account for a mean of ∼0.7 mag and ∼0.4 mag of extinction, respectively, to provide accurate distance measurements, which in consequence are sensitive to the uncertain nature of extragalactic reddening laws.

Wide-scale follow-up of Cepheids in the near-infrared (NIR), to mitigate dust effects, first became practical with WFC3/IR, allowing measurements at 1.6 μm and reducing the mean impact of extinction to ∼0.1 mag and the sensitivity to reddening laws (Riess et al. 2011). However, the advantage of NIR observations over optical bands came with new challenges; at these wavelengths, the resolution of HST is 2–3 times lower and the background (in the form of ubiquitous red giants) is an order of magnitude greater. The lower resolution at NIR leads to an increase in the photometric errors of individual Cepheid measurements (after the systematic bias is statistically removed using artificial star tests), which may limit the precision (from random error) of distance measurements

without a large number (>50) of Cepheids in each host. While Cepheid distance measurements from either the optical or NIR are in good agreement (R22), a result most likely if both are accurate, the pursuit of a 1% measurement of the Hubble constant demands ever more stringent tests of Cepheid photometry.

The newly launched James Webb Space Telescope (JWST) offers the twin advantages of angular resolution comparable to the great visible-light resolving power of HST WFC3/UVIS and the lower impact of interstellar dust as WFC3/IR in the same observation. JWST observations planned for its first GO cycle have been designed to take advantage of these capabilities and reobserve Cepheids previously measured with HST, work that is likely to require years to collect and thoroughly analyze to fully come to fruition. However, an early observation with JWST of an SN Ia host previously observed by HST, though not dedicated for this purpose, offers a valuable preview.

To be clear in setting expectations for future JWST observations, these archival observations of the Cepheids in NGC 1365 fall short of demonstrating the full capability of the observatory for this endeavor. They are shorter in exposure time by a factor of a few than those planned for this purpose and they are obtained at nearly twice the wavelength needed to optimally resolve and reduce the contributions of nearby red giants (i.e., the background). Notably, they cover a more crowded region along a spiral arm (see Figure 1) compared to most of those observed by HST. Further, they provide only a single (i.e., "random") epoch or phase in each Cepheid light curve, which adds an additional dispersion of 0.1 to 0.2 mag depending on the amplitude of the Cepheid. Finally, the state of the JWST calibration data (e.g., flat fields, dark frames, bias frames, geometric distortion maps, linearity corrections) is in its first iteration and will improve with time. Nevertheless, and with these limitations in mind, these observations preview the enhanced capabilities of JWST over HST and provide meaningful, if preliminary, quantitative results.

In Section 2 we describe the details of the JWST observations for NGC 1365, as well as the data reduction and photometry procedures. We show our results in Section 3 and give a brief discussion in Section 4. An Appendix provides information about past HST observations of Cepheids in NGC 1365 for easy reference.

2. Observations, Data Reduction, and Photometry

2.1. Observations and Data Reduction

The central region of NGC 1365 was recently observed with JWST NIRCam on 2022 August 13 as part of program GO-2107 (PI: Janice Lee), which aims to study the star formation activity in 19 nearby galaxies. The NGC 1365 field partially overlaps with an HST WFPC2 time-series field (GO-5972, PI: Jeremy Mould) where dozens of Cepheids were discovered (Silbermann et al. 1999; Hoffmann et al. 2016) and followed up in the NIR (R22). With the Cepheid locations and periods determined from those HST data, we have an opportunity to photometer and study these Cepheids in the new JWST observations. In Figure 1 we show the footprints of the JWST observations as well as archival HST observations and locations of previously identified Cepheids. The initial WFPC2 time series and WFC3 follow-up targeted a less-crowded part of the host off the spiral arms, but the NIRCam observations targeted the center of the galaxy and primarily contain Cepheids in a small dense, crowded region. Figure A1 shows less-crowded Cepheids imaged by HST that are more similar to those typically studied in HST fields. Due to the overlap of the two observatories, we can also directly compare the images and measurements of many of the same Cepheids in the denser regions of the host.

We retrieved JWST observations of NGC 1365 from MAST and processed the raw data (stage 0) using the JWST Science Calibration Pipeline version 1.6.2. There are 25 exposures in total, with the short-wavelength channel through the F200W filter and the long-wavelength channel through the F300M, F335M, and F360M filters. In this study, we only analyzed the F200W data for their depth and proximity in wavelength coverage compared to the HST F160W band. The F200W data consist of eight subfields, with each one covered by approximately one short-wavelength detector. Only the two eastmost subfields contain previously identified Cepheids; thus, we excluded the other six from the analysis. The total exposure times are 1202.52 s for both analyzed subfields.

We noticed the $1/f$ noise causing small bias shifts in the calibrated stage 2 data products (see Section 2 of Merlin et al. 2022). We corrected them by subtracting the median value of each row and then each column before the JWST pipeline stage 3 process. Similar to Merlin et al. (2022), we masked all sources when computing the median values for row and column subtractions.

We used the WCS in the images to locate the Cepheids based on their HST positions. We identified a global shift of $\sim 0\farcs5$ between the HST and JWST positions and accounted for this to register the images. After this global shift we found point sources at the expected positions of the Cepheids to a precision of less than a NIRCam pixel ($0\farcs031$; see Figure 2). The HST NIR observations in these spiral arms are undersampled (even after drizzling to $0\farcs08\,\mathrm{pixel}^{-1}$ resolution) and lack the inherent resolution of JWST (despite the greater wavelength of those observations).

While the Cepheids were easily apparent in the deeper and higher-resolution images in F200W, they were hard to discern in the accompanying observations at longer wavelengths and through medium-width bands due to their much shorter exposure times, lower angular resolution, and lower throughput of these filters. As a result we only analyzed the F200W images.

2.2. Photometry

We performed point-spread function (PSF) photometry using a crowded-field photometry package based on DAOPHOT/ALLSTAR Stetson (1987, 1994). We constructed an empirical model of the PSF using F200W observations of the standard star P330E (taken on 2022 August 29, obs. ID = jw01538o155t002) obtained in a 160-pixel subarray (using a minimal exposure time to keep the star below saturation) that included two dithers placed on each of the B-module chips. At this time, the observations of P330E are the only ones within the appropriate characteristics (including timing and pointing) to be used for this effort. P330E is a G2V star (Bohlin & Landolt 2015) with similar colors as Cepheids, and has been used for Cepheid photometric calibration across previous SH0ES analyses.

We chose not to use the pipeline calibration to obtain the image zero-points as they have been found to have limited accuracy (at the time of this writing) including chip-to-chip

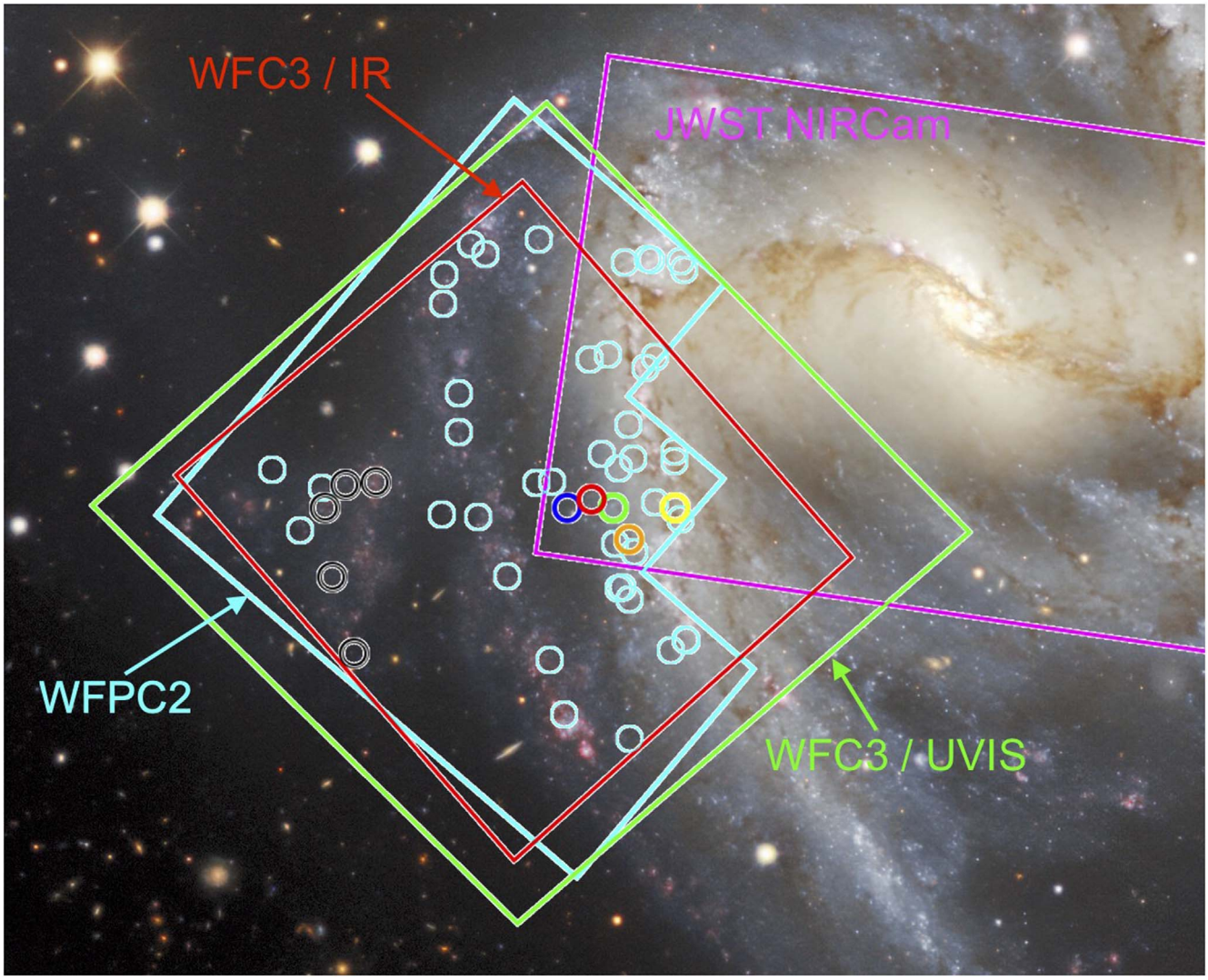

Figure 1. Observation footprints of NGC 1365 with JWST NIRCam (magenta), HST WFPC2 (cyan), WFC3/UVIS (green), and WFC3/IR (red) overlaid on a color composite image from the Dark Energy Survey (DOE/FNAL/DECam/CTIO/NOIRLab/NSF/AURA). The locations of Cepheids used in this study are indicated by circles. North is up, and east is to the left.

offsets (and possible time dependence between the early life of the mission and the present; Boyer et al. 2022; Brammer 2022; Nardiello et al. 2022). To produce reliable zero-points for the observation of NGC 1365 we used the above observations of P330E obtained and combined for each B-module chip separately to directly calibrate the Cepheids observed in that chip. We assigned each image of P330E a reference Vega magnitude of 11.42 mag (Rieke et al. 2022). An important advantage of using the 2022 August 29 observations of P330E to set the zero-points for the images of NGC 1365 is that they were obtained only 2 weeks after the observation of NGC 1365, an interval during which JWST's wave front monitoring has shown it to be relatively stable with modeled photometric variations over the interval of <0.01 mag (M. Perrin, 2022 private communication). (We did not make use of aperture photometry for the Cepheids due to the inability to separate nearby sources as expected from inspection of Figure 2.)

To avoid a flux bias from the determination of Cepheid positions in HST NIR images, it is necessary to fix their locations using the uncrowded optical images (i.e., "forced photometry"; Riess et al. 2009). The algorithm fits the PSF of the Cepheids at their known, fixed positions, subtracts them from the images, identifies additional, unresolved sources down to a fixed threshold, and then simultaneously optimizes the fit to the non-Cepheids (parameters are x, y, and flux) and Cepheids (parameter is flux) to determine the latter's flux. We then add "artificial stars" at the same brightness as the Cepheid (based on the period and iterative fit of the period–luminosity (P-L) relation), and remeasure these using the same procedure to account for the mean background of unresolved sources near the position of the Cepheid (i.e., a statistical crowding correction) and to measure the uncertainty in the Cepheid magnitude. The photometry results are given in Table 1. We also compared our results to the level 3, full-calibrated images produced by the STScI pipeline and found that the photometry was consistent between the versions of the images.

3. Results

Fixing the slope of the P-L relation to the global value of -3.30 determined from the mean of thousands of Cepheids in the MW, Large Magellanic Cloud, Small Megellanic Cloud,

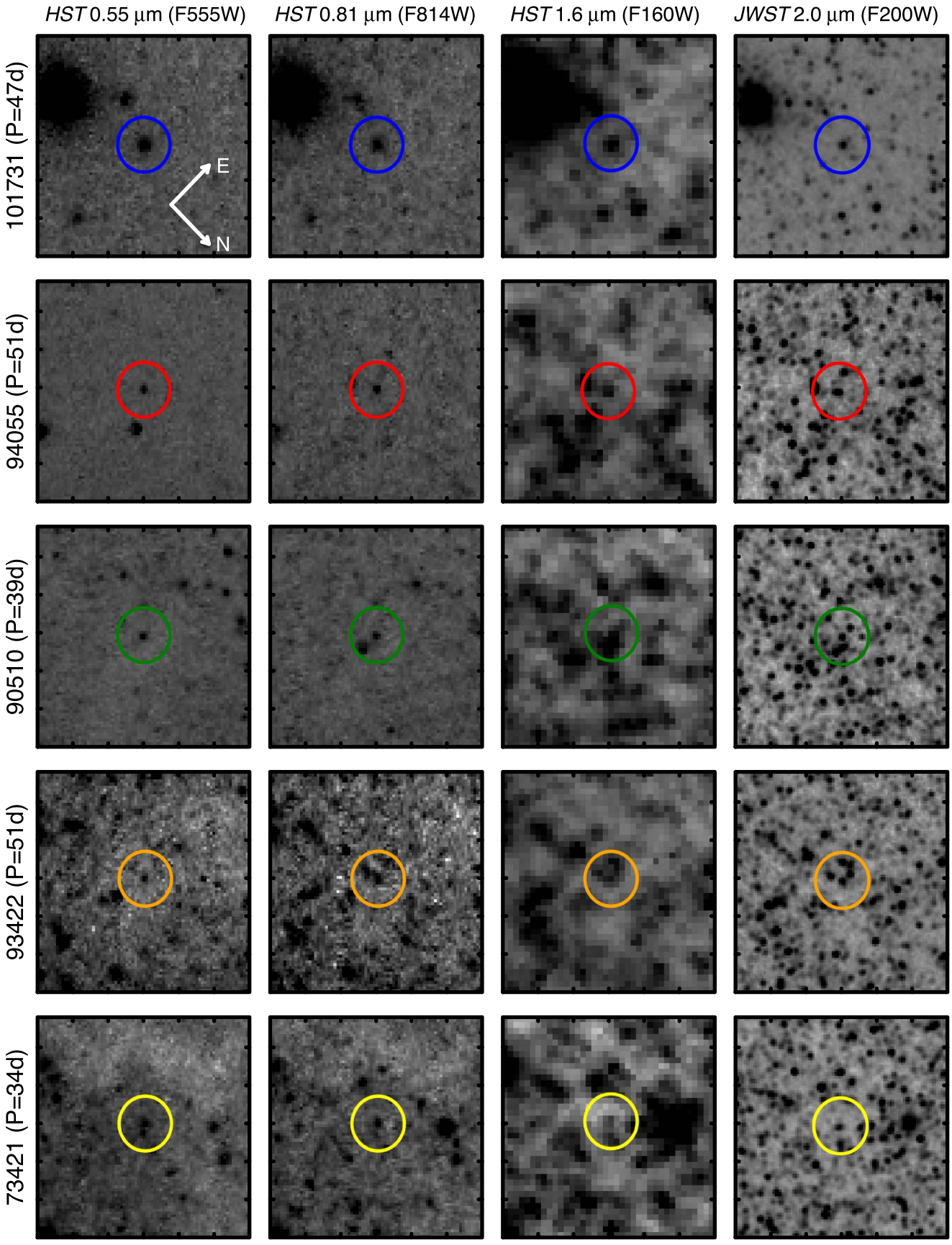

Figure 2. Image cuts of five example Cepheids analyzed in this study. Their locations are indicated by the corresponding colors in Figure 1. The circles cover a radius of $0\farcs375$, while the image cuts display $3''$ on a side. From left to right, each row shows one (same) Cepheid in HST F555W, F814W, F160W, and JWST F200W, where the exposure times are 1410 s, 1770 s, 3618 s, and 1203 s, respectively. The orientation of the image cuts is indicated by the white compass in the top left panel.

Table 1
JWST F200W Cepheid Photometry

ID	P (days)	F200W [a] (mag)	σ [b]	R.A. [c] (deg) (J2000.0)	Decl.	Subfield
97917	24.00	24.64	0.32	53.433156	−36.158061	south
60205	25.30	24.44	0.36	53.435680	−36.144208	south
25668	26.13	24.38	0.51	53.432499	−36.136873	north
74699	26.58	24.67	0.46	53.427052	−36.156193	south
40364	27.48	23.90	0.39	53.429580	−36.143996	south
65664	29.34	24.74	0.35	53.431935	−36.149101	south
53380	30.85	24.32	0.40	53.433946	−36.143847	south
100027	31.37	24.34	0.21	53.439120	−36.153423	south
79315	31.46	24.15	0.31	53.432884	−36.152400	south
80300	32.38	24.44	0.32	53.434414	−36.151327	south
94995	32.42	23.87	0.31	53.431335	−36.158716	south
45761	33.03	24.45	0.44	53.430433	−36.144804	south
73421	33.50	23.60	0.33	53.427504	−36.155372	south
61628	37.01	23.25	0.28	53.427674	−36.151793	south
17203	38.12	24.24	0.43	53.430027	−36.136683	north
90510	39.06	23.65	0.24	53.433311	−36.155466	south
77265	39.61	24.24	0.27	53.429382	−36.154908	south
58983	39.67	24.32	0.29	53.427627	−36.151066	south
101731	47.24	22.96	0.19	53.437542	−36.155483	south
8616	48.09	22.85	0.33	53.427309	−36.136727	north
9712	48.33	23.41	0.29	53.426932	−36.137379	north
93422	51.34	23.38	0.23	53.431778	−36.157790	south
94055	51.45	23.56	0.18	53.435355	−36.154809	south
17544	51.94	23.56	0.24	53.430280	−36.136566	north

Notes.
[a] These are Vega mag referenced to P330E = 11.42 in F200W.
[b] The errors are derived from artificial stars and also include a random phase error in quadrature of 0.15 mag.
[c] Positions are referenced to the WCS of JWST images processed using JWST pipeline v1.6.2.

M31, NGC 4258, and SN Ia hosts in the NIR (R22), we measured the intercepts at $\log P = 1$.

For our "baseline," we limited the comparison to a period range of $1.35 < \log P < 1.75$ where the Cepheids as measured from both telescopes have strong signal-to-noise ratios. Below this range the signal-to-noise ratio at $F160W = 24.5$ (Vega) drops to <10 and above this range Cepheid periods in NGC 1365 are not expected to be accurate because the original time series used to find the Cepheids in NGC 1365 spanned only 48 days ($\log P = 1.68$), so that a full cycle would not have been seen. The JWST and HST Cepheid P-L relations are shown in Figure 3.

For JWST with PSF fitting (referenced to P330E) and with 24 Cepheids we find an intercept of 25.75 ± 0.06 (SD = 0.36 mag). In Table 2 we provide intercepts for broader ranges of periods.

To directly compare the HST and JWST P-L relations observed at different, though adjacent, bandpasses, it is necessary to account for their different wavelength responses. Due to the simple spectral energy distributions of stars, particularly on the Rayleigh–Jeans tail in the NIR, it is relatively straightforward to estimate this difference, which is the color F160W–F200W, from another measured color such as F555W–F814W. To do this rigorously we used the PARSEC isochrones (Bressan et al. 2012) for stellar atmospheres that are provided as calculated for the HST and JWST bandpasses (using version CMD v3.6).[4] We limited these to a range appropriate for Cepheids: ages of 10–100 Myr, $T_{\rm eff}$ of 4000°–7000°, initial masses $>3M_{\odot}$, and $\log g < 2$. These stars have a tight locus in the color–color plane of WFC3/UVIS for F555W–F814W versus F160W(HST)–F200W (JWST). We fit a second-order polynomial to the color–color relation, finding

$$F160W - F200W = 0.008 + 0.052(F555W - F814W) + 0.078(F555W - F814W)^2.$$

The dispersion of the synthetic values around this approximation is 0.007 mag. The mean Cepheid color of the sample is $F555W - F814W = 1.08$ mag (sample SD = 0.22 mag) where the relation gives F160W − F200W = 0.15 mag (sample SD = 0.05 mag); however, we computed the individual values for each Cepheid, as given in the Appendix. We subtract the individual F160W–F200W colors predicted from the optical colors from the measured HST F160W to provide a direct comparison to JWST F200W as shown in Figure 3.

The baseline measurements of the HST intercepts use the F160W magnitudes as given in R22, the F160W–F200W colors as given in the Appendix, and include 38 Cepheids in this period range. To increase the sample for the purpose of this HST to JWST comparison, we added the three Cepheids with $P = 51$, 51, and 52 days found by Hoffmann et al. (2016) and only slightly above the $P < 50$ day limit used by R22 but still well below the 1.2× time span of the observations necessary to be reliable. We find an intercept for HST at $\log P = 1$ of 25.75 ± 0.05 mag for this sample of 41 Cepheids. We also tested other period ranges and provide their resultant intercepts in Table 2.

[4] http://stev.oapd.inaf.it/cgi-bin/cmd

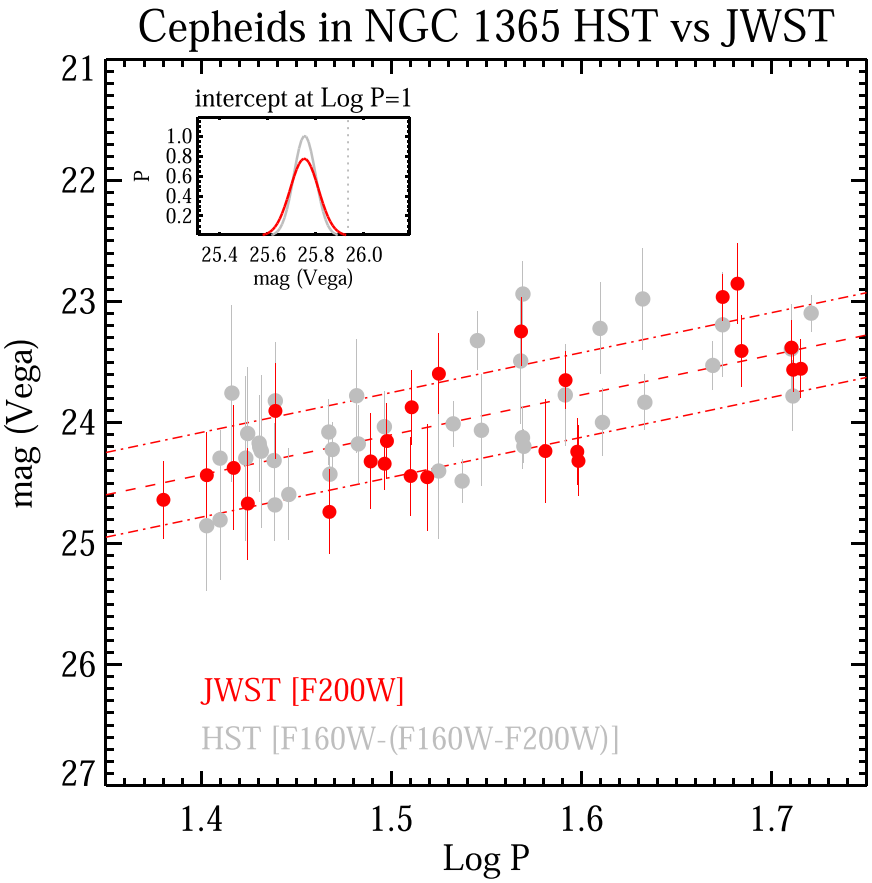

Figure 3. Near-infrared period–luminosity relations for Cepheids in the range $1.35 < \log P < 1.75$ (baseline results) measured with HST and JWST. The JWST sample (red) includes 24 Cepheids observed in F200W (2μm). The HST sample includes 38 Cepheids from R22 with F160W magnitudes transformed to F200W using a color transformation based on their measured F555W–F814W colors and F160W–F200W. The inset shows the intercepts of the relations at $\log P = 1$. The solid red curve uses the JWST PSF photometry calibrated to P330E.

Table 2
HST and JWST Intercepts at $\log P = 1$ (slope $= -3.30$) for NIR Cepheids in NGC 1365

Sample	*N* Cepheids	Period Range	F200W Intercept[a]
HST WFC3/IR field, baseline	**38**	**$1.35 < \log P < 1.75$**[c]	**25.754 ± 0.045**
HST WFC3/IR field, extended	49	$1.15 < \log P < 1.75$	25.736 ± 0.043
HST WFC3/IR field, SH0ES R22[b]	46	$15.0 < P < 50.0$	25.750 ± 0.045
JWST NIRCam field, baseline, PSF	**24**	**$1.35 < \log P < 1.75$**[c]	**25.752 ± 0.059**
JWST NIRCam field, extended, PSF	31	$1.15 < \log P < 1.75$	25.718 ± 0.055

Notes.
[a] Results from HST measured in F160W and converted to F200W using $\mathrm{F160W} - \mathrm{F200W} = 0.008 + 0.052(\mathrm{F555W} - \mathrm{F814W}) + 0.078(\mathrm{F555W} - \mathrm{F814W})^2$.
[b] Same period range and sample used in R22.
[c] The bold entries indicate our baseline results for HST and JWST, respectively.

The inset in Figure 3 compares the intercepts. The agreement between the HST and JWST intercepts is very good, below 1σ in their difference.[5] A similar mean difference is seen when comparing the Cepheids measured by both HST and JWST; however, this sample is far smaller ($N = 10$) and thus the comparison is less significant. The dispersion around the P-L relation as shown in Figure 3 is comparable between HST and JWST and is likely to be smaller for optimal JWST observations with multiple epochs, better image calibration, and in less-crowded regions more typically observed with HST.

To a $\sim$0.05 mag level of preliminary accuracy based on still limited characterization of JWST and for this case, we can conclude that past HST NIR measurements do not appear biased, let alone "biased bright" at the $\sim$0.2 mag level (i.e., by the systematics of past photometry measurements or by previously unresolved companions) as could mitigate the "Hubble tension" in R22 (and then only if such a bias was not also similarly present in HST photometry of Cepheids in the geometric anchor, NGC 4258).

[5] The small size of the offset between baseline intercepts appears coincidental given the random error in the intercepts of $\sim$0.05 mag and $\sim$0.06 mag for HST and JWST, respectively. The offsets of the extended samples are larger at 0.02 mag.

4. Discussion

The JWST images and measurements of Cepheids in NGC 1365 and in comparison to those from HST bode well for the quality of such future measurements. We reiterate that these observations were not optimized for observing Cepheids and are far from the best that JWST can do. Optimal observations would be longer in exposure time, cover multiple passbands to the necessary depth, include shorter wavelengths for better resolution, include multiple epochs to reduce the random phase noise, have higher signal-to-noise calibration frames (flats, darks, bias frames, chip offsets, geometric distortion for locating Cepheids, etc.) available, and better cover the regions where past HST programs have found Cepheids and measured their periods.

We also note that it is too early in the life of JWST and NIRCam to identify and calibrate subtle photometric effects. There is one such effect we are aware of, the count-rate nonlinearity (CRNL), which makes faint objects appear fainter, though the scale of this effect has been diminishing with improvements in NIR detector manufacturing and testing used to select the best chips. Because the level of CRNL has not yet been measured in space for NIRCam, we did not correct either the NIRCam or the WFC3/IR Cepheid photometry for this effect, so to first approximation we might expect that CRNL cancels in the comparisons provided here. For WFC3/IR, CRNL makes the Cepheids in NGC 1365 ∼0.03 mag faint relative to the flux level of standard stars (Riess et al. 2009). If the CRNL of NIRCam is ∼half the level of WFC3/IR (our guess), the error in the comparison will be ∼0.015 mag, negligible at the precision of *this* study, but important to calibrate for future, larger samples. The single-epoch sampling of this JWST observation introduces a statistical bias of ∼0.005 mag in the Cepheid P-L relation compared to the typical flux-averaged (multiepoch) observations. This bias is again negligible for the precision of this study.

Nevertheless, the quantitative comparison of the first JWST Cepheid P-L intercepts presented here is promising, and already significant as a check on past HST measurements. Based on what we have seen for sparser HST fields, we expect a scatter of ∼0.20–0.25 mag for optimal JWST observations, about 50% smaller than this nonideal case. We also expect that the calibration of this observatory will only improve and mature, leading to future observations that should provide ever more definitive investigations.

We are indebted to all of those who spent years and even decades bringing JWST to fruition. We are grateful to the proposers of GO-2107 (PI: Janice Lee) for making their program nonproprietary, enabling the community to undertake assorted investigations from this data including this study. We thank the anonymous referee for providing constructive suggestions and improving the paper. This research made use of the NASAs Astrophysics Data System.

Appendix
Cepheid Measurements from HST

In Table A1, we list the previously measured HST F160W photometry and colors for the Cepheids in NGC 1365 for easy reference. Figure A1 shows five examples of less crowded Cepheids imaged by HST that are more similar to those typically studied in HST fields.

Table A1
HST F160W Cepheid Photometry

ID	P	F160W	σ	F555W−F814W	F160W−F200W	R.A.[a]	Decl.
	(days)			(mag)		(deg) (J2000.0)	
60205	25.16	25.03	0.54	1.18	0.18	53.435572	−36.144146
136735	25.57	24.41	0.23	0.89	0.12	53.465135	−36.152743
43927	25.57	24.98	0.50	1.17	0.17	53.440450	−36.135135
101154	25.94	23.89	0.73	0.98	0.13	53.426225	−36.165263
106082	26.38	24.40	0.68	0.84	0.11	53.432670	−36.161386
74699	26.44	24.28	0.55	1.23	0.19	53.426941	−36.156136
63449	26.81	24.39	0.40	1.35	0.22	53.445400	−36.136227
138773	26.83	24.35	0.21	1.04	0.15	53.462525	−36.157297
101112	26.88	24.37	0.63	0.98	0.13	53.426292	−36.165183
120972	27.30	24.46	0.31	1.04	0.15	53.443078	−36.160625
126914	27.33	24.78	0.30	0.80	0.10	53.455397	−36.153646
40364	27.34	23.94	0.48	0.91	0.12	53.429471	−36.143937
65336	27.79	24.71	0.38	0.89	0.12	53.446800	−36.135500
124631	29.17	24.22	0.27	1.02	0.14	53.438970	−36.166817
130859	29.21	24.56	0.24	0.98	0.13	53.458170	−36.153817
133465	29.29	24.44	0.23	1.34	0.22	53.460423	−36.154001
105797	30.17	23.98	0.47	1.28	0.20	53.431618	−36.162206
106470	30.23	24.30	0.32	0.93	0.12	53.427648	−36.166054
100027	31.20	24.11	0.29	0.66	0.08	53.439011	−36.153369
73421	33.32	24.52	0.56	0.91	0.12	53.427399	−36.155314
122163	33.91	24.20	0.19	1.23	0.19	53.449210	−36.155957
139368	34.28	24.64	0.18	1.09	0.16	53.459369	−36.160824
87703	34.92	23.51	0.24	1.22	0.19	53.449343	−36.140061
117850	35.09	24.21	0.46	1.04	0.15	53.445830	−36.156138
61628	36.80	23.79	0.52	1.63	0.30	53.427562	−36.151741
103387	36.88	24.25	0.26	0.94	0.12	53.447790	−36.146777
80315	36.90	23.12	0.27	1.20	0.18	53.449213	−36.137887

Table A1
(Continued)

ID	P (days)	F160W	σ	F555W−F814W (mag)	F160W−F200W	R.A.[a]	Decl. (deg) (J2000.0)
142648	36.94	24.32	0.14	0.93	0.12	53.457318	−36.166545
90510	38.84	23.92	0.42	1.05	0.15	53.433201	−36.155411
128912	40.51	23.39	0.38	1.14	0.17	53.437587	−36.170953
103704	40.63	24.24	0.28	1.43	0.24	53.440403	−36.153516
104907	42.66	23.14	0.42	1.11	0.16	53.432245	−36.161310
123489	42.77	23.96	0.23	0.95	0.13	53.431458	−36.172785
109560	46.44	23.80	0.20	1.54	0.27	53.447707	−36.149730
101731	46.99	23.31	0.43	0.90	0.12	53.437427	−36.155425
93422	51.07	23.65	0.37	1.49	0.26	53.431666	−36.157737
94055	51.17	24.00	0.29	1.35	0.22	53.435250	−36.154750
134975	52.31	23.21	0.15	0.88	0.11	53.460099	−36.155567

Note.
[a] Positions are referenced to the WCS of HST F160W images processed using `AstroDrizzle` v2.2.6.

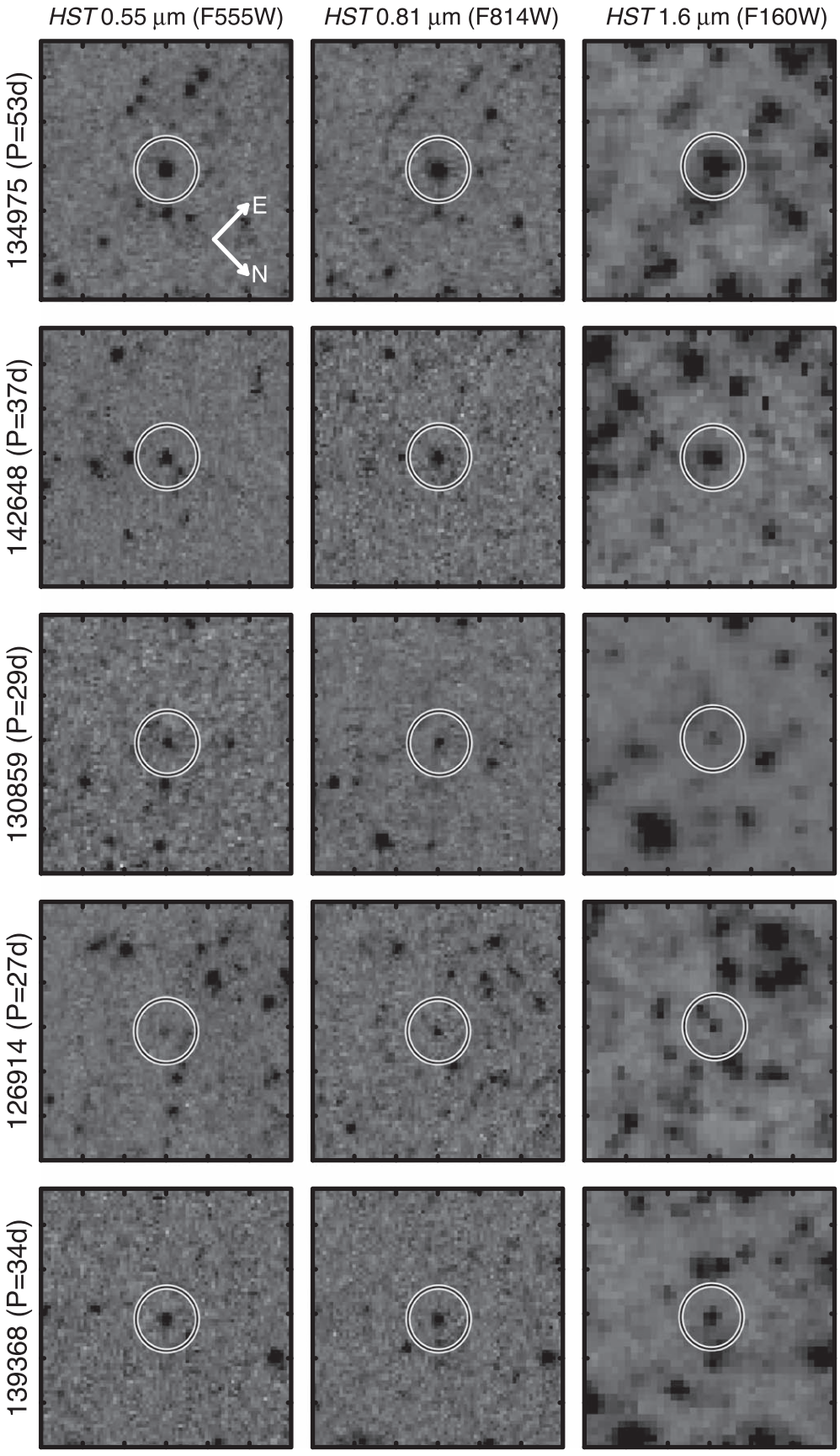

Figure A1. Same as Figure 2, but for five examples in the more typical, lower-density HST F160W field, where JWST observations are not available. See Figure 1 for locations.

ORCID iDs

Wenlong Yuan https://orcid.org/0000-0001-9420-6525
Adam G. Riess https://orcid.org/0000-0002-6124-1196
Lucas M. Macri https://orcid.org/0000-0002-1775-4859

References

Bohlin, R. C., & Landolt, A. U. 2015, AJ, 149, 122
Boyer, M. L., Anderson, J., Gennaro, M., et al. 2022, RNAAS, 6, 191
Brammer, G. 2022, grizli, v1.5.0, Zenodo, doi:10.5281/zenodo.5012699
Bressan, A., Marigo, P., Girardi, L., et al. 2012, MNRAS, 427, 127
Cruz Reyes, M., & Anderson, R. I. 2022, arXiv:2208.09403
Eddington, A. S. 1927, MNRAS, 87, 539
Freedman, W. L., Madore, B. F., Gibson, B. K., et al. 2001, ApJ, 553, 47
Hoffmann, S. L., Macri, L. M., Riess, A. G., et al. 2016, ApJ, 830, 10
Leavitt, H. S., & Pickering, E. C. 1912, HarCi, 173, 1
Macri, L. M., Stanek, K. Z., Bersier, D., Greenhill, L. J., & Reid, M. J. 2006, ApJ, 652, 1133
Merlin, E., Bonchi, A., Paris, D., et al. 2022, ApJ, 938, L14
Nardiello, D., Bedin, L. R., Burgasser, A., et al. 2022, MNRAS, 517, 484
Rieke, G. H., Su, K., Sloan, G. C., & Schlawin, E. 2022, AJ, 163, 45
Riess, A. G., Breuval, L., Yuan, W., et al. 2022a, ApJ, 938, 36
Riess, A. G., Macri, L., Casertano, S., et al. 2009, ApJ, 699, 539
Riess, A. G., Macri, L., Casertano, S., et al. 2011, ApJ, 730, 119
Riess, A. G., Yuan, W., Macri, L. M., et al. 2022b, ApJL, 934, L7
Sandage, A., Tammann, G. A., Saha, A., et al. 2006, ApJ, 653, 843
Silbermann, N. A., Harding, P., Ferrarese, L., et al. 1999, ApJ, 515, 1
Stetson, P. B. 1987, PASP, 99, 191
Stetson, P. B. 1994, PASP, 106, 250